3-D Electrostatic Hybrid Element Model for SAW Interdigital Transducers

Carlos F. Jerez-Hanckes, *Student Member, IEEE*, Vincent Laude, *Member, IEEE*, Jean-Claude Nédélec, and Raphael Lardat

***Abstract*—In this work, the singular behavior of charges at corners and edges on the metallized areas in SAW transducers are investigated. In particular, it is demonstrated that a tensor product of the commonly used Tchebychev bases overestimates the singularities at corners, and, hence, it cannot be used in a proper boundary element method formulation. On the other hand, it is shown that a simple finite element method-like approach is impractical due to the enormous number of unknowns required to model the electrode's large length-to-width ratio. These considerations are then used for defining a hybrid element model, which combines Tchebychev and linear polynomials over differently meshed domains. Such an approach is shown to suitably account for charge singularities while greatly reducing the number of unknowns. Results are obtained for isotropic and anisotropic substrates for non-periodic configurations.**

I. Introduction

From an early stage in their development, interdigital transducers (IDTs) have been known to suffer from diffraction losses at the electrodes' ends and junctions [1], [2]. The diffraction is provoked by the uneven distribution of electrical charges at the corners of the structure: a fundamental difference to the regularity displayed by the edge charges. In fact, this edge behavior is responsible for the generation of the desired surface acoustic waves (SAWs) [3]. As a result of the charge inhomogeneity, the quests for ever narrower acoustic beam widths and ever lower energy consumption are hindered: hence the need for a complete model of the electric behavior of the transducer.

The electromechanical equations involved are simplified by the so-called quasi-static approximation [4], which separates the electric field from the magnetic one. From it, a direct relation between the potential and the charge distribution is derived; if either of them is known, an accurate electrostatic model—one that also embodies the anisotropy of the substrate—can be obtained. More often than not, approaches rely on the knowledge of the applied potential; the charges are obtained by analytic and/or numerical schemes, which are specially efficient when the piezoelectric surface is not entirely metallized. Furthermore, the electrodes-bus system can be electrostatically pictured as flat surfaces, as the charges at the metal/piezoelectric interface account for the generation of acoustic waves. However, this does not circumvent the three-dimensional (3-D) nature of the problem. Lastly, unless specified, we will assume the electrodes and buses to be perfect conductors.

Previous efforts for simulating the surface charge distribution over IDTs can be classified according to their nature: 2-D or 3-D; analytic or numerical; and within the last category, upon the function bases used. In 2-D models, the problem is assumed to be invariant along the electrodes' length. In this case, several analytic solutions were developed, most of them using complex function theory [5], [6]. Numerically, some of the models comprise expansions in pulse functions as in [2], [7], the solutions being found by the method of moments (MoM) for a differential functional and by point-matching techniques, respectively. However, the most adequate way to describe the line charge distribution in the electrode/substrate interface is given by [8]

$$\sigma(y) = \sum_n \sigma_n \frac{T_n(y/a)}{\sqrt{1-(y/a)^2}}, \tag{1}$$

where a is the electrode's half-width and $T_n(\cdot)$ is the first-kind Tchebychev polynomial of order n. Since these polynomials accurately describe the singular behavior of $\sigma(y)$ at the edges of 2-D electrodes, very few of them are required (3 to 5) compared to those required in the step function approximation. This improvement has been used in the construction of hybrids of the boundary and finite element methods (BEM and FEM) as in [9], [10]. Nonetheless, 2-D models are not capable of describing the diffraction phenomena previously mentioned.

In 3-D space, complete analytic solutions are no longer available except for a small number of simple geometries, and therefore we rely only on numerical approaches, sometimes simplified by questionable premises. In [11], the authors assumed that the signal was not distorted by diffraction, and consequently the actual charge distribution $\sigma(x, y)$ was averaged over the aperture, thereby rendering a 2-D model. In [3], pulse function expansions were solved by the MoM for an artificial boundary problem periodic in both directions. This was done in order to deal with the finiteness of the structure along the transversal

Manuscript received January 15, 2007; accepted September 28, 2007.

C. F. Jerez-Hanckes and V. Laude are with the Département LPMO of the Institut Franche-Comté Electronique Mécanique Thermique et Optique-Science et Technologie (FEMTO-ST), Centre National de la Recherche Scientifique UMR 6174, F-25044 Besançon, France (e-mail: carlos.jerez@polytechnique.edu).

C. F. Jerez-Hanckes and J.-C. Nédélec are with the Centre de Mathématiques Appliquées, Centre National de la Recherche Scientifique UMR 7641, Ecole polytechnique, F-91128 Palaiseau, France.

C. F. Jerez-Hanckes and R. Lardat are with Temex, Sophia-Antipolis, F-06904, France.

Digital Object Identifier 10.1109/TUFFC.2008.693

direction. Although not an accurate picture for a single IDT, singularities were retrieved at the end points of the electrodes, from where excitation of Rayleigh waves is expected. Finally, in [12]–[14] vertex charge inhomogeneities were revealed by means of a pulse basis expansion, where the generated linear system was solved by a collocation method. Unfortunately, the implementation of pulse functions demands a large number of variables due to their inadequacy in representing the singular charge behavior. Thus, based on the success that the Tchebychev basis provided for 2-D models, great improvement in SAW modeling is to be expected if the singular behaviors are embedded in the basis functions.

This article is organized as follows: in Section II, we present several results concerning the asymptotic behavior of charges at corners and edges for flat perfect conductors; in Section III, a hybrid element model is described which enforces the edge behavior and approximates singularities at vertices by a linear FEM-like basis; and finally, preliminary results are discussed for different material configurations for non-periodic structures.

II. Charge Distributions at Edges and Corners

In perfect conductors, electrical charges present two distinct features: they distribute exclusively over the surface, thereby defining a surface charge density, and they exhibit singularities at the edges and corners of the material [15]. Nonetheless, these singularities are subject to the so-called edge condition: the energy density must be integrable over any finite domain [16], [17]. More accurately, the electromagnetic energy density in any finite domain Ω must be finite,

$$\int_{\Omega} \left(|\mathbf{E}|^2 + |\mathbf{H}|^2\right) d\Omega < \infty, \tag{2}$$

where $\mathbf{E}$ and $\mathbf{H}$ represent the electric and magnetic fields, respectively. The surface charge distribution σ is proportional to the normal electric field,

$$\sigma \;\propto\; \mathbf{E}\cdot\hat{n} = -\frac{\partial\phi}{\partial n}. \tag{3}$$

In what follows, it will be assumed that the analysis is carried out in the neighborhood of the edge or vertex, i.e., in a region of small radius with respect to all relevant wavelengths, so that low frequency techniques may be applied [18]. Depending on whether the domain and the boundary conditions are translationally invariant along one axis or not, the problem can be stated in two or three dimensions. Furthermore, our analysis will be focused on the case of flat electrodes, since it is assumed that the electrical interaction between the conductors and the piezoelectric material occurs only at the substrate surface.

A. Edges

An edge is characterized by local invariance in one coordinate, as shown in Fig. 1, i.e., the edge is locally straight.

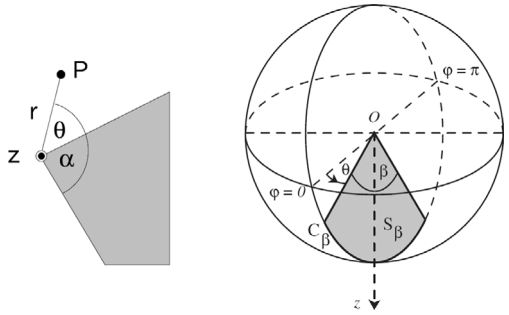

Fig. 1. Local coordinate systems used for the asymptotic analysis at an edge (left) and at a flat sector vertex (right).

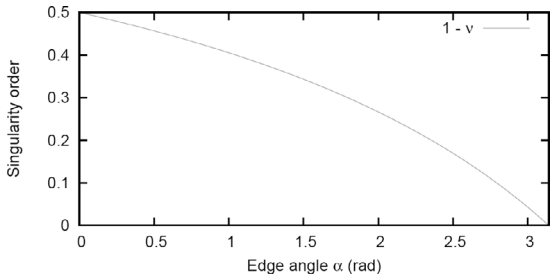

Fig. 2. Singularity curve for $\alpha \in [0, \pi]$. As the angle becomes less acute, the singularity weakens.

Let z follow the direction of the edge, then the potential can continuously be expressed in cylindrical coordinates as

$$\phi(r,\theta,z) = r^{\nu}\left[a_0(\theta,z) + r a_1(\theta,z) + r^2 a_2(\theta,z) + \dots\right]. \tag{4}$$

This equation holds only outside the conductor, as the potential on the conductor is constant—in our case, equal to zero. It is well known [16] that, for two faces intersecting at an angle $\alpha \in (0,\pi)$, the surface charge density has an asymptotic—lowest order—behavior given by

$$\sigma(r,\theta,z) \;\sim\; \frac{1}{r^{1-\nu}}, \qquad \nu = \frac{\pi}{2\pi - \alpha}, \tag{5}$$

where (4) has been replaced in (3).

Fig. 2 shows the decrease in the singular exponent with α, the most singular case occuring for infinitely thin edges, $\alpha = 0$ and $\nu = 1/2$. This result validates the Tchebychev polynomials (1) approach for describing the electrodes: let the edges be located at $x_1 = \pm a$, and let d be the distance from either edge to x_1; then $d = |a - x_1|$ and

$$\begin{aligned}\sigma(d) &= \frac{T_n(1-d/a)}{\sqrt{1-(1-d/a)^2}} \\ &= \frac{aT_n(1-d/a)}{\sqrt{2ad-d^2}} \;\sim\; \frac{C(d)}{\sqrt{d}},\end{aligned}$$

which reveals the aforementioned behavior.

At this point, we could consider approximating the charges over a rectangular conductor—a single electrode—by tensorial products of Tchebychev polynomials:

$$\sigma(x,y) \;\stackrel{?}{=}\; \sum_{m,n} \sigma_{mn} \frac{T_n(x/a)}{\sqrt{1-(x/a)^2}} \frac{T_m(y/b)}{\sqrt{1-(y/b)^2}}, \tag{6}$$

where a, b are equal to half the dimensions of the rectangle. At any edge sufficiently far from the vertices, the approximation is valid, the demonstration being equivalent to the one shown before. At a corner, however, we must regard the behavior as the lowest-order approximation. Let us introduce the local polar coordinates (r, θ), measured from any of the vertices $(\pm a, \pm b)$:

$$x = \pm a - r\cos\theta, \qquad y = \pm b - r\sin\theta.$$

The lowest order occurs for n, $m = 0$. Hence, for r tending to zero,

$$\sigma(r,\theta) = \frac{\sqrt{ab}}{r\sqrt{\cos\theta\sin\theta}} \times \left[4 - 2r\left(\frac{\cos\theta}{a} + \frac{\sin\theta}{b}\right) + \frac{r^2}{ab}\cos\theta\sin\theta\right]^{-1/2}.$$

After a Taylor expansion for the term in square brackets, we find

$$\sigma(r,\theta) \approx \frac{\sqrt{ab}}{r\sqrt{\cos\theta\sin\theta}}\left(\frac{1}{2} + O(r)\right).$$

If we fix r, then the singular behavior is as $1/\sqrt{d}$, where d is the distance to the edge given by either $r\sin\theta$ or $r\cos\theta$ when θ approaches 0 or $\pi/2$, respectively. On the other hand, for a fixed angle, it shows a $1/r$ behavior. Such singularity is non-integrable over the surface, as it yields a divergent potential in $\log r$, and, therefore, our guess in (6) turns out to be invalid. This compels us to regard the entire 3-D local space at corners.

B. Corners

To describe the neighborhood of a flat corner, most authors [18]–[20] use spherical coordinates, as in Fig. 1, although the sphero-conal system has also been used [21]. The potential is locally given by

$$\phi(R,\theta,\varphi) = R^{\nu}V(\theta,\varphi). \tag{7}$$

From (3), the surface charge distributes as

$$\sigma \sim R^{\nu-1}. \tag{8}$$

By separation of variables, an eigenfunction problem is formulated for the angular function: $V(\theta,\varphi)$ satisfies Laplace's equation on the conducting sector S, of angle β, with an homogeneous Dirichlet condition over the boundaries C. Mathematically,

$$\begin{aligned}\Delta_S V(\theta,\varphi) + \nu(\nu+1)V(\theta,\varphi) = 0 \quad &\text{over } S,\\ V(\theta,\varphi) = 0 \quad &\text{over } C,\end{aligned}$$

where

$$\Delta_S\, u = \frac{1}{\sin^2\theta}\frac{\partial^2 u}{\partial\varphi^2} + \frac{1}{\sin\theta}\frac{\partial}{\partial\theta}\left(\sin\theta\,\frac{\partial u}{\partial\theta}\right)$$

is the Laplace-Beltrami operator. When $\beta = \pi$, the angular sector is a half-plane given by $\varphi = 0$, which is also $\varphi = 2\pi$, and $V(\theta,\varphi)$ is given by spherical harmonics that vanish at $\varphi = 0, 2\pi$. This case is equivalent to the local behavior at an edge, as the smallest eigenvalue is $\nu = 1/2$. For other angular sectors, solutions can only be found numerically through variational techniques [22] or via the Wentzel-Kramers-Brillouin (WKB) method [21]. From the cited works, the asymptotic behavior for corner angles $\pi/2$ and $3\pi/2$ are approximately

$$\nu_{90} \approx 0.296\,584 \quad \Rightarrow \quad \sigma_{90} \sim \frac{1}{R^{0.703416}}, \tag{9a}$$

$$\nu_{270} \approx 0.814\,655 \quad \Rightarrow \quad \sigma_{270} \sim \frac{1}{R^{0.185345}}. \tag{9b}$$

More generally, the singularity exponent in modulus is smaller or larger than 1/2, depending on the reentrant or salient nature of the corner, respectively. No analytical solution can be found for these values; separation of cartesian variables cannot be employed for modeling charge distributions at corners.

From a SAW modeling perspective, two possible approaches are at hand: (i) define local polar coordinates for every corner and establish the appropriate angular functions; or (ii) approximate charges by interpolating functions over small elements surrounding the vertex. Although more rigorous than (ii), solution (i) requires the solving of complex issues such as function definition, determination of valid domains, and computation of solutions at intersecting domains, all of which have to be dealt with for every geometry considered. On the other hand, (ii) requires only the choice of interpolating functions, avoiding all other problems, for which reason it will be the approach taken.

Singular interpolating functions were used in [23], where the authors model the surface charge density via a Galerkin formalism that uses continuous second-order basis for smooth areas, and defines special singular elements according to the different angles encountered. This approach requires fewer elements than in a zero-order or first-order approximation but the element integral calculations become more complicated; the integrals are hypersingular for self-terms. For a wisely refined mesh, the vertex areas can still be approximated by simpler functions such as first-order polynomials, as in common FEM formulations. Unluckily for the case of SAW IDTs, this alternative on its own demands a number of degrees of freedom (DOF) beyond any practical use, as discussed further below.

III. Hybrid Elements Model

From the above analysis, and always assuming flat perfect conductors, we propose the following model:

- The metallized area Ω is divided in two subdomains: Ω_T, which takes most of the electrodes' areas, and

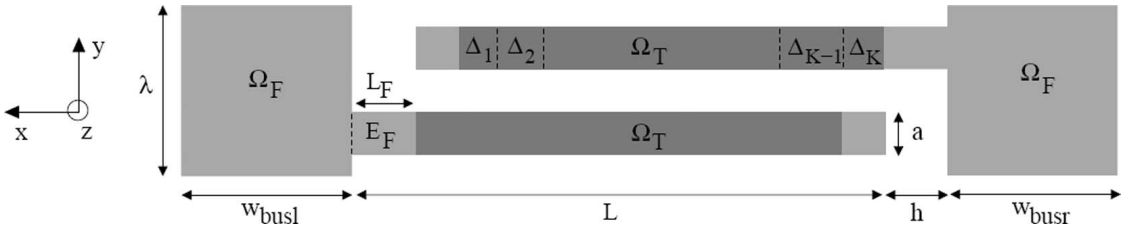

Fig. 3. Parameters and regions used in the hybrid element model for a single IDT period. Dark gray areas are triangularly meshed, whereas light gray regions correspond to Tchebychev-pulse solution subdomains.

Ω_F, which corresponds to the remaining domain, i.e., $\Omega_F = \Omega \setminus \Omega_T$. These areas are depicted in Fig. 3.

- Each of the rectangular areas, corresponding to the number of electrodes N_c, in Ω_T is divided into K stripes of width Δ_k, where the charges are modeled by Tchebychev polynomials T_n, $0 \le n \le N_{Tch}$, multiplied by their weight function. N_{Tch} is the maximum polynomial order to be used. The solution at the stripe k, on the c-th electrode, is given by

$$\sigma_{ck}(x,y) = \sum_{n=0}^{N_{Tch}} \sigma_{ckn} \frac{T_n(y_c)}{\sqrt{1-y_c^2}} \sqcap (x_k^c) \sqcap (2y_c), \tag{10}$$

where $x_k^c = (x - X_k^c)/\Delta_k$ and $y_c = (y - Y_c)/a^c$. Y_c is the y-coordinate of the c-electrode's center, a^c is its half-width, and X_k^c is the central x-coordinate of the k-th stripe at that same electrode. The function $\sqcap(x)$ is defined as

$$\sqcap(x) = \begin{cases} 1 & |x| \le \frac{1}{2} \\ 0 & |x| > \frac{1}{2} \end{cases}.$$

Using the above, the solution over Ω_T can be written as

$$\sigma_T(x,y) = \sum_{c=1}^{N_c} \sum_{k=1}^{K} \sigma_{ck}(x,y). \tag{11}$$

The choice of pulse functions along the electrodes' length is justified by the fact that the edge charges distribute in a regular fashion. Nonetheless, other bases could be equally implemented such as Fourier-basis or higher-order polynomials.

- Ω_F is triangularly meshed so as to approximate the solution by classic FEM-type first-order ($\mathbb{P}_1$) polynomials [24], i.e.,

$$\sigma_F(x,y) = \sum_{e=1}^{N_F} \sum_{j=1}^{3} \sigma_j^e N_j^e(x,y), \tag{12}$$

where N_F is the total number of elements in Ω_F and $N_j^e(x,y)$ is the j-th linear interpolating function of the e-th element.

With these approximations, the complete charge distribution $\sigma(x,y)$ over Ω is obtained by solving the Fredholm integral equation of the first kind:

$$\phi(x,y) = \int_\Omega G(x,y;x',y')\,\sigma(x',y')\,dx'dy', \tag{13}$$

where $\sigma(x,y)$ is the unknown, $\phi(x,y)$ is the known applied potential, and $G(x,y;x',y')$ is the electrostatic Green's function. This function may represent an isotropic or anisotropic material, a nonperiodic [25] or periodic structure [13], without changing the formulation of the problem. It is numerically solved by a variational scheme: multiplying (13) by a test function σ^t and integrating over Ω yields

$$\int_\Omega \phi(x,y)\,\sigma^t(x,y)dxdy = \int_\Omega \int_\Omega G(x,y;x',y')\,\sigma(x',y')\,\sigma^t(x,y)\,dx'dy'.$$

By replacing the test function for the different approximations, we calculate self-terms and cross terms. When in Ω_T, the test function chosen is

$$\sigma_T^t(x,y) = \frac{T_n(y_c)}{\sqrt{1-y_c^2}} \sqcap [x_k^c] \sqcap [2y_c] \tag{14}$$

for all $n = 0, \ldots, N_{Tch}$, $k = 1, \ldots, K$, and $c = 1, \ldots, N_c$. For Ω_F, the tests functions σ_F^t are

$$\sigma_F^t(x,y) = N_j^e(x,y)$$

for all $j \in \{1,2,3\}$ and $1 \le e \le N_F$. Notice that a global node numbering system is necessary afterwards. Through this formulation, a discrete system is built of the form

$$\begin{pmatrix} M_{FF} & M_{FT} \\ M_{FT}^t & M_{TT} \end{pmatrix} \begin{pmatrix} \sigma_F \\ \sigma_T \end{pmatrix} = \begin{pmatrix} \phi_F \\ \phi_T \end{pmatrix}, \tag{15}$$

where the resulting matrix M is symmetric, due to the form of the kernel—Green's function—and, consequently, the number of terms to be found is reduced by half. Furthermore, this formulation does not require the imposition of matching conditions at the boundaries of the different elements; they occur naturally. Opposingly, collocation techniques require the enforcement of matching conditions.

IV. Results and Discussion

A. Model Validation

To validate our model, we first compare analytic results to those obtained by first-order approximations. Once we have established the accuracy of the $\mathbb{P}_1$ approximation, we assess the proposed hybrid elements model.

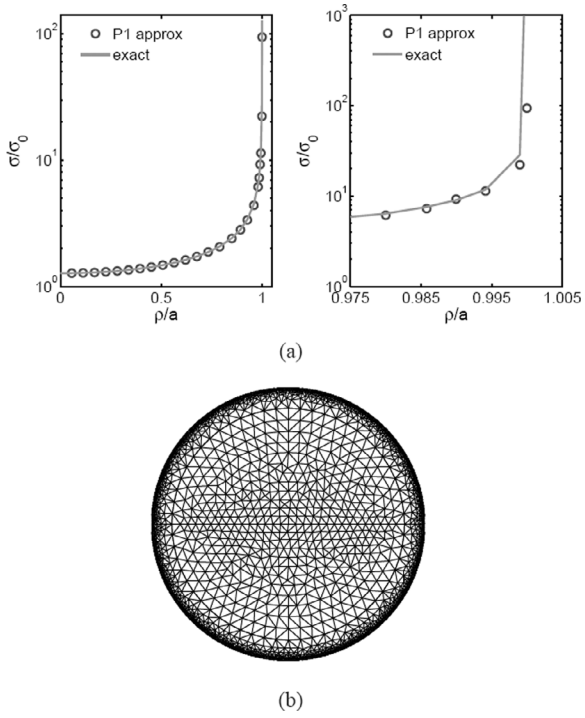

Fig. 4. First-order approximation and exact solution for the normalized charge distribution over a disk of radius a. A highly refined mesh made of 2997 nodes has been used. (a) Normalized charge distributions. (b) Used mesh.

1. First-Order Approximations: Let us consider the charge distribution over a perfectly conducting disk of radius a and zero thickness, surrounded by an isotropic medium. The system is governed by the classic 3-D Poisson's equation whose Green's function is

$$G(\rho, z, z') = \frac{1}{4\pi\epsilon\sqrt{\rho^2 + (z - z')^2}}, \tag{16}$$

where $\rho = \sqrt{(x - x')^2 + (y - y')^2}$. For a constant applied potential, we know that the charge density is given by [26]

$$\sigma = \sigma_0 / \sqrt{1 - (\rho/a)^2},$$

where σ_0 is a dimensional quantity proportional to the potential. For a numerical approximation, we mesh the disk following the method in [27], where it was shown that, for edge and corner singularities, optimal meshes can be achieved when refinement is given by a $h^{1/(1-\nu)}$ rule, h being obtained from the diameter of the circle inscribed in each triangle. If the domain is meshed as described, the convergence rate of the first-order approximation is proportional to h. Adaptive meshing can be implemented with commercial meshers or free ones such as FreeFem++ [28], our choice for this work. Fig. 4 shows the mesh used, for which $\nu = 1/2$, and the close agreement between our results and the analytic behavior up to 99.95% of the radius. Closer to the edge, the calculations lose accuracy as a consequence of the discrete nature of the approximation.

2. Hybrid Element Method vs. First-Order Approximations: In Fig. 5, we obtain the normalized charge distribution contours for a perfectly conducting flat rectangle. Since no analytic solution is available, we compare solutions given by solely $\mathbb{P}_1$ approximations [Fig. 5(a)] and the hybrid elements model [Fig. 5(b)], where the center of the rectangle is modeled by Tchebychev polynomials. Overall, both solutions behave equally, but the number of variables required for the hybrid approach is already 60% that of the $\mathbb{P}_1$ approximation, proving the validity of the proposed model. Further on, it will be shown that the economy in degrees of freedom increases proportionally with the electrode length. On the other hand, the number of Tchebychev quadrature points required for matrix term computations is inversely proportional to the mesh parameter h, in order to compensate for the large size of the stripes compared to the triangular elements. Hence, there is a need for optimal meshing strategies such as those described below.

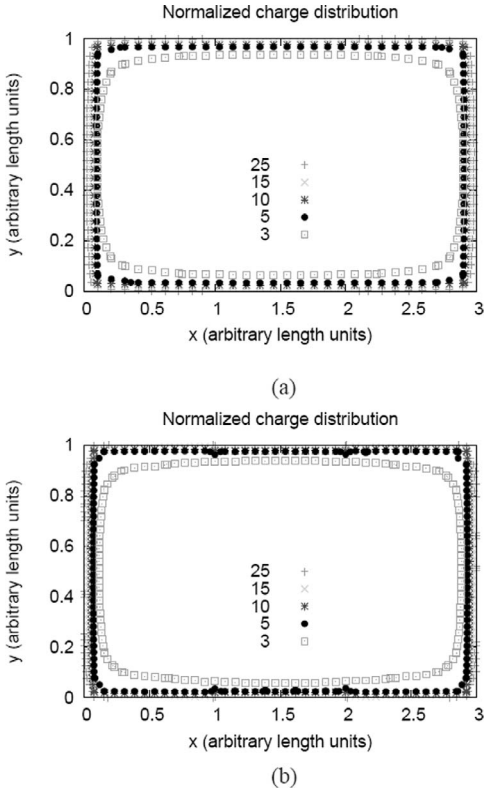

Fig. 5. Contour plots for (a) $\mathbb{P}_1$ and (b) hybrid bases approximation of the normalized charge distribution over a flat rectangle with length to width ratio 3:1; (a) required 4939 variables, whereas (b) required only 3191 nodes in the triangular mesh and 90 degrees of freedom in the Tchebychev region, for a total of 3281 degrees of freedom. (a) $\mathbb{P}_1$ approximation solution. (b) Mixed element solution.

B. Mesh Design

The mesh used for representing Ω_F directly influences the calculation time and the accuracy of the solution. On the one hand, the number of nodes in Ω_F must be sufficient to smoothly describe the singularities and also allow for a correct matching between the FEM solution and the Tchebychev profiles at the boundary with Ω_T.

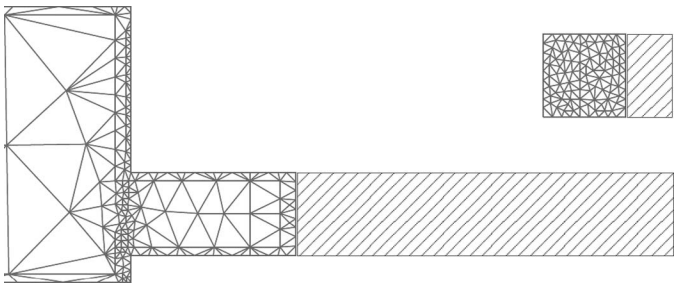

Fig. 6. Section of Ω_F meshed. Refinement toward the edges and corners is necessary for accuracy. Striped areas define the electrodes' belonging to Ω_T.

On the other hand, the number of matrix term computations increases as N_F^2 and as N_F^3 for solving the linear system if classic algorithms are applied. A balanced meshing strategy consists of defining an interior region, $\Omega_i \not\subseteq \Omega_F$, coarsely meshed, and refining the remaining areas closer to the borders of Ω_F. This approach proved to reduce the number of unknowns while keeping an adequate degree of freedom for accounting for singularities. An example of the resulting mesh is presented in Fig. 6.

For a suitable match between $\mathbb{P}_1$ and Tchebychev elements, a certain distance from a corner singularity is necessary. Consider the neighborhood of a reentrant corner given by an electrode-bus intersection. Let E_F denote the electrode region in Ω_F containing the angle, i.e., $E_F \subset \Omega_F$, of dimensions $a \times L_F$. The mesh surrounding the corner is given by the interplay between the length of E_F, and the width and position of the first stripes in Ω_T. This is explained as follows: as we move away from the reentrant corner, a transition occurs from the lower-order singularity toward the ubiquitous $[1 - y_c^2]^{-1/2}$ edge singularity. Since the last behavior is imposed in Ω_T, mesh and stripe refinement are needed to smoothly describe the change. In this regard, two approaches are at hand, depending on the length of E_F, L_F:

1) if large compared to the electrode width a, as seen in Fig. 6, the transition occurs almost solely in Ω_F, and all stripes can be much wider than the closest triangular mesh elements;
2) if smaller than a, stripes near Ω_F must have widths comparable to the neighboring triangular elements in Ω_F so as to continue the transition.

In either case, mesh refinement is necessary around the vertex, as previously discussed. Notice that a singularity transition region is always required, and, therefore, we cannot place Ω_T just after the bus. For salient corners, these issues also apply.

C. Isotropic Electrostatic Green's Function

As a first test for our model, we consider a single pair of opposing electrodes, placed over the surface of an isotropic half-infinite substrate in contact with vacuum. For this, we use a non-periodic, isotropic Green's function, found as the solution for Laplace's equation at the interface between two materials at $z = z' = 0$:

$$G_{iso}(\bar{x}, \bar{y}) = \frac{1}{2\pi\epsilon_0(1+\epsilon_r)} \frac{1}{\sqrt{\bar{x}^2 + \bar{y}^2}}, \tag{17}$$

where $\bar{x} = x - x'$, $\bar{y} = y - y'$, and ϵ_0 is the vacuum permittivity.

Fig. 7(a) shows the surface charge distribution for a single electrode-bus cell placed over a GaAs substrate ($\epsilon_r = 9.735$). The electrodes are 60λ long, the metallization ratio is 0.7, the bus widths are equal to 15λ, the bus-electrode gap is equal to 1.5λ, and the applied voltages are ± 1 V. Fig. 7(b) and (c) display the singularities presented by reentrant corners as seen in (9b), and by salient vertices as observed in (9a), respectively. Moreover, they reveal the accurate matching between the different approximations at the common boundaries of Ω_F and Ω_T. The solutions found at the nodes must be interpreted as average values over surface elements, and, hence, do not reflect the infinities that should be found if their values were taken exactly at the boundaries. From the solutions obtained, capacitances due to charge build-up at the borders of the conductors can be estimated.

For equal electrode-bus dimensions and applied potential modulus, a positively (negatively) charged bus-electrode system is observed to be the inverse reflection of the negative (positive) one. Notwithstanding, inside each electrode, charges are more concentrated at the facing sides of the electrode pair than at the outer ones. This asymmetry is caused by the non-periodic nature of the kernel and should disappear for the periodic case [13].

As expected, great economy is made by approximating the electrodes by Tchebychev bases over stripes instead of using $\mathbb{P}_1$ bases over a meshed domain. Let us denote by N_v^e the number of nodes at any of the borders between Ω_F and Ω_T, and α the ratio between the length of the electrode L and the central wavelength λ. Assuming a uniform mesh, a lower limit for the number of nodes that would be required to model a single electrode in Ω_T is approximately given by

$$N_v^e \times \frac{L}{a} N_v^e = (N_v^e)^2 \frac{2\alpha}{MR},$$

where MR is the metallization ratio $a/p = 2a/\lambda$ for a single electrode period. As an example, for the simulation presented in Fig. 7(a), where $N_v^e = 10$, if we had meshed Ω_T, the number of variables would have been proportional to

$$N_c(N_v^e)^2 \frac{2\alpha}{MR} = 2 \times (10)^2 \times \frac{2 \cdot 60}{0.7} \approx 4 \times 10^4,$$

whereas the number of Tchebychev variables accounts for only $N_c \times K \times (N_T + 1) = 800$, where N_T is the maximum Tchebychev polynomial order and N_c is the total number of electrodes. This yields a reduction in number of unknowns of 50 times, which translates into a saving of 2500 times less matrix elements to compute.

TABLE I

COMPUTATION TIMES FOR THE ISOTROPIC CASE FOR DIFFERENT PARAMETER VALUES ($\lambda = 2\ \mu$M, $a/p = 70\%$) AT SIMILAR ACCURACIES.

Run	Electrode length (λ)	Bus width (λ)	N_{FEM}	K	N_{Tch}	N_{GT}	N_{GL}	Total DOF	Time (min.)
A	60	15	959	100	3	16	5	1759	7.29
B	60	15	959	60	3	14	7	1439	5.01
C	60	15	959	40	3	14	7	1279	3.27
D	100	20	1341	200	3	16	5	2941	27.58
E	100	20	1341	300	1	16	5	1841	18.13
M2	80	15	940	200	3	14	4	2540	16.28
M2-O	80	15	940	30	3	14	7	1180	2.49

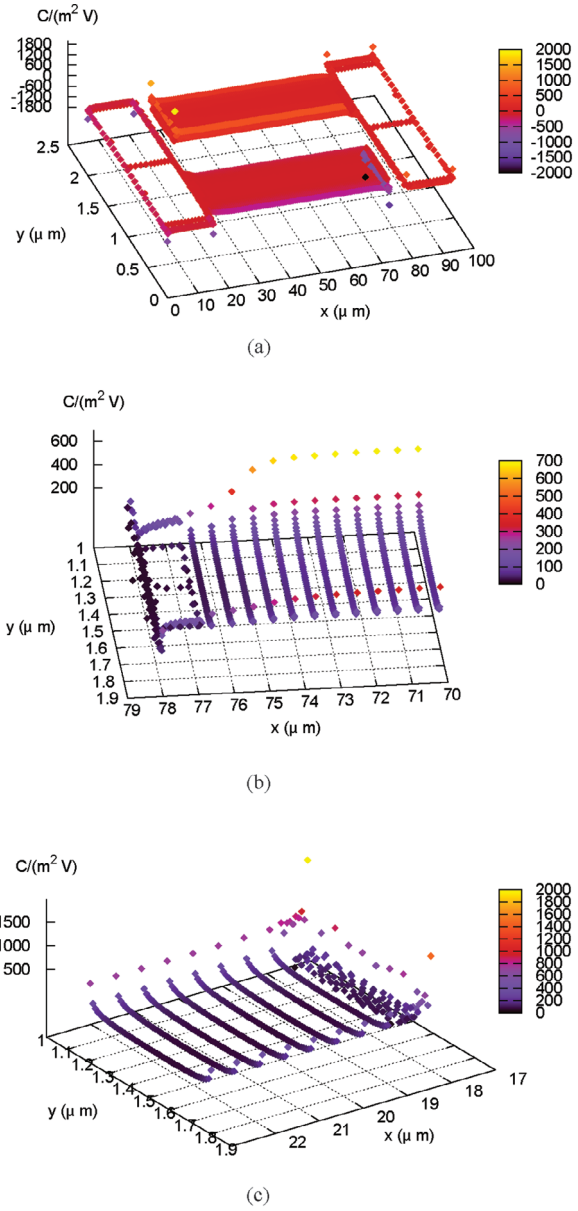

Fig. 7. Surface charge distribution for an isotropic Green's function corresponding to a GaAs substrate. Charges are scaled in ϵ_0. (a) Overall charge distribution. (b) Charge density at the positive electrode-bus junction. At the reentrant corner, the singularity is small in comparison to the one at the edges, as theoretically expected. (c) Positive electrode tip. Charge density increases at the side facing the opposite electrode, and large peaks are observed at salient vertices.

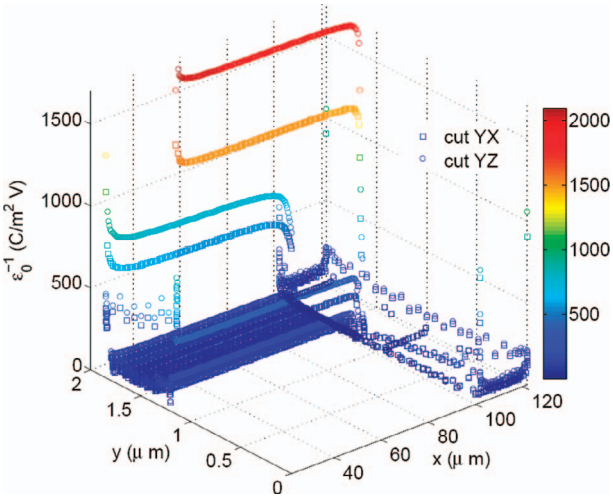

Fig. 8. Comparison of surface charge distributions for cuts YX (square markers) and YZ (circle markers) for LNO. Equal simulation parameters were used: $K = 200$, $N_F = 1075$, $N_{Tch} = 3$, $N_{GL} = 4$, and $N_{GT} = 18$.

In the present case, the kernel-test function integrals are solved by semi-analytic expressions in order to accelerate the calculation. The resulting expressions are then solved by either Gauss-Tchebychev or Gauss-Legendre quadratures, the choice depending on the weight function in the integral. Due to small differences found between the matrix elements, m_{ij} and m_{ji}, we have chosen to calculate all elements, and symmetrize the resulting matrix. This certainly slows computation times but assures the best convergence, and further improvement is to be expected. With this in mind, several calculation times are shown in Table I, where variations for electrode length, polynomial order, bus width, stripe number K, and number of terms used in Gauss-Tchebychev (N_{GT}) and Gauss-Legendre quadratures (N_{GL}) are exposed. Although for a purely electrostatic case the wavelength has no influence over the solutions, we have parametrized dimensions in λ in order to reflect dimensions usually found in SAW transducers.

The simulations presented were selected upon agreement with fundamental electrostatics as well as interface matching. For instance, when there is poor meshing, positive values at nodes can be found at the negative electrode and vice versa. This incongruency is due to the lack of nodes, as linear interpolation will not properly model

singularity curves. Matching was analyzed by defining a threshold for the differences between different approximations at the interface.

From Table I, consistency with common 2-D simulations is retrieved by the small values of N_{Tch} used for obtaining acceptable solutions. For simulations A-E, all stripes are equidistant, i.e., $\Delta_k = \Delta = L/K$, the bus-electrode spacing is equal to 1.5λ, and the meshes used are of the type shown in Fig. 6. For runs A-C, the exact same mesh was used but with different values for K and N_{GT}. It is observed that, as K diminishes, the variable N_{GL}, associated with width quadrature along the stripe, must be increased in order to account for wider stripes, so as to provide sensible results. Simulation A corresponds to the solution shown in Fig. 7. For simulations D and E, electrode length and bus width were increased, thereby requiring more unknowns, K and N_F, and thus accounting for large computation times. The factor of two increase in processing time between simulations D and E reveals the impact that N_{Tch} has on computation time. Thus, accurate solutions can be obtained by refining stripe width and reducing N_{Tch}, and, consequently, diminishing computation time as well. Hence, further time reduction can be expected by adaptively defining stripe widths and polynomial order.

In runs M2 and M2-O, the mesh was changed so that Ω_T is closer to the buses, and the bus-electrode spacing is equal to λ. As previously discussed, the proximity of the stripes in such a case is crucial for convergence. In M2, 200 equidistant stripes were required for solving the 80λ electrode, whereas in M2-O an uneven stripe spacing following Tchebychev zeros yielded better matching results for only 30 stripes and reduced computation time by a factor of 6.5.

D. Anisotropic Electrostatic Green's Function

Although the isotropic case allows us to validate and analyze several issues concerning the proposed hybrid element method, the model's utility relies on the ability to portray anisotropic media. In this case, the vacuum/anisotropic substrate Green's function is given by

$$G_{ani}(\bar{x},\bar{y}) = \frac{1}{2\pi\epsilon_0}\Big[\sqrt{\bar{x}^2+\bar{y}^2} + \sqrt{\epsilon_n\bar{x}^2 + 2\epsilon_p\bar{x}\bar{y} + \epsilon_m\bar{y}^2}\Big]^{-1}, \quad (18)$$

where the following parameters are defined in terms of the relative permittivities of the substrate:

$$\epsilon_m = \epsilon_{11}\epsilon_{33} - \epsilon_{13}^2 > 0,$$
$$\epsilon_n = \epsilon_{22}\epsilon_{33} - \epsilon_{23}^2 > 0,$$
$$\epsilon_p = \epsilon_{12}\epsilon_{33} - \epsilon_{13}\epsilon_{23}.$$

Notice that, in the isotropic case, we recover (17).

In Fig. 8 we present positive electrode-bus charge distributions for two different cuts of lithium niobate (LNO): YZ ($\epsilon_{11} = 23.25$, $\epsilon_{22} = \epsilon_{33} = 40.32$), and YX ($\epsilon_{11} = \epsilon_{33} = 40.32$, $\epsilon_{22} = 23.25$) [29], which correspond to two cases for $\epsilon_p = 0$: anisotropic, $\epsilon_m < \epsilon_n$, and isotropic, $\epsilon_m = \epsilon_n$, respectively. Physically speaking, the second case is equivalent to placing the electrodes at an angle of 90° with respect to their position in the first scenario, the YZ-cut. The electrode considered has a length of 80 μm, a width of .7 μm, a bus width of 20 μm, and an electrode-bus spacing of 2 μm. It is clear that the anisotropy modifies the charge profiles: for the YZ-cut, the overall charge concentration is greater than for the YX case. Moreover, values at the edges have relative increases larger than those at the corners. This is explained by the smaller dielectric constant along the y direction, accounting for profiles different from those found in isotropic cases.

From a computational point of view, the same considerations given for the isotropic case hold. However, the anisotropy in the kernel function requires special attention along those axes where the dielectric constant is smaller. This is due to the weight the dielectric terms have on the integral equation, and, thus, mesh optimization should take into account this preference.

V. Conclusions

We have discussed the singular behavior at the edges and corners of flat conductors. While Tchebychev approximations at edges prove to be adequate, analytic solutions at the corners are discarded. A hybrid element approach is proposed, using Tchebychev and linear interpolating polynomials, where the integral equation is solved variationally, and results for isotropic and anisotropic non-periodic Green's function validate the model. The method shows to be in accordance with theoretical results as well as with previous models, while greatly reducing the number of unknowns. Future work comprises enhanced optimization to reduce computation time and the implementation of the full piezoelectric Green's function.

Acknowledgments

The authors thank Dr. Natacha Béreux, Dr. Thomas Pastureaud, and Dr. William Steichen for their fruitful conversations and advice.

References

[1] R. Milsom, N. Reilly, and M. Redwood, "Analysis of generation and detection of surface and bulk acoustic waves by interdigital transducers," *IEEE Trans. Sonics Ultrason.*, vol. 24, no. 3, pp. 147–166, 1977.

[2] R. Wagers, "Transverse electrostatic end effects in interdigital transducers," in *Proc. IEEE Ultrason. Symp.*, 1976, pp. 536–539.

[3] R. Wagers, "Analysis of finite-width interdigital transducers excitation profiles," *IEEE Trans. Sonics Ultrason.*, vol. 26, no. 2, pp. 105–111, 1979.

[4] D. Royer and E. Dieulesaint, *Ondes Élastiques dans les solides.* vol. 1, Paris: Masson, 1996.

[5] B. Abbott and C. Hartmann, "An efficient evaluation of the electrostatic fields in IDTs with periodic electrode sequences," in *Proc. IEEE Ultrason. Symp.*, 1993, pp. 157–160.

[6] S. Biryukov and V. Polevoi, "The electrostatic problem for the SAW interdigital transducers in an external electric field—Part I: A general solution for a limited number of electrodes," *IEEE Trans. Ultrason., Ferroelect., Freq. Contr.*, vol. 43, no. 6, pp. 1150–1159, 1996.

[7] A. Baghai-Wadji, S. Selberherr, and F. Seifert, "On the calculation of charge, electrostatic potential and capacitance in generalized finite SAW structures," in *Proc. IEEE Ultrason. Symp.*, 1984, pp. 44–48.

[8] V. Plessky and T. Thorvaldsson, "Periodic Green's function analysis of SAW and leaky SAW propagation in a periodic system of electrodes on a piezoelectric crystal," *IEEE Trans. Ultrason., Ferroelect., Freq. Contr.*, vol. 42, no. 2, pp. 280–293, 1995.

[9] P. Ventura, J. M. Hodé, and B. Lopes, "Rigorous analysis of finite SAW devices with arbitrary electrode geometries," in *Proc. IEEE Ultrason. Symp.*, 1995, pp. 257–262.

[10] J. Ribbe, "On the Coupling of Integral Equations and Finite Elements/Fourier Modes for the Simulation of Piezoelectric Surface Acoustic Wave components," Ph.D. thesis, Centre de Mathématiques Appliquées, École Polytechnique, Palaiseau, France, 2002.

[11] B. Lewis, P. Jordan, R. Milsom, and D. Morgan, "Charge and field superposition methods for analysis of generalized SAW interdigital transducers," in *Proc. IEEE Ultrason. Symp.*, 1978, pp. 709–714.

[12] A. Baghai-Wadji, S. Selberherr, and F. Seifert, "Rigorous 3D electrostatic field analysis of SAW transducers with closed-form formulae," in *Proc. IEEE Ultrason. Symp.*, 1986, pp. 23–28.

[13] H. Bachl and A. Baghai-Wadji, "3D electrostatic field analysis of periodic two-dimensional SAW transducers with closed-form formulae," in *Proc. IEEE Ultrason. Symp.*, 1989, pp. 359–362.

[14] H. Zidek and A. Baghai-Wadji, "Proposed elemental charge distributions in finite-aperture SAW-device models," *Electron. Lett.*, vol. 30, no. 11, pp. 915–917, 1994.

[15] J. Jackson, *Classical Electrodynamics*. 3rd ed. New York: John Wiley & Sons, Inc., 1998.

[16] J. Meixner, "The behavior of electromagnetic fields at edges," *IEEE Trans. Antennas Propagat.*, vol. 20, no. 4, pp. 442–446, 1972.

[17] A. Heins and S. Silver, "The edge conditions and field representation theorems in the theory of electromagnetic diffraction," in *Proc. Cambridge Philosoph. Soc.*, vol. 51, 1955, pp. 149–161.

[18] J. Van Bladel, *Singular Electromagnetic Fields and Sources*. IEEE Press Series in Electromagnetic Wave Theory. Piscataway, NJ: IEEE Press, 1991.

[19] M. Costabel and M. Dauge, "Singularities of electromagnetic fields in polyhedral domains," *Arch. Rational Mech. Anal.*, vol. 151, pp. 221–276, 2000.

[20] J. Keller, "Singularities at the tip of a plane angular sector," *J. Math. Phys.*, vol. 40, no. 2, pp. 1087–1092, 1999.

[21] A. Abawi, R. Dashen, and H. Levine, "The eigenvalues of the Laplacian on a sphere with boundary conditions specified on a segment of a great circle," *J. Math. Phys.*, vol. 38, no. 3, pp. 1623–1649, 1997.

[22] R. De Smedt and J. Van Bladel, "Field singularities near aperture corners," in *Proc. IEEE*, vol. 134, pp. 694–698, 1987.

[23] D. Greenfield and M. Monastyrski, "Three-dimensional electrostatic field calculation with effective algorithm of surface charge singularities treatment based on the Fichera's theorem," *Nucl. Instrum. Methods Phys. Res. A*, vol. 519, pp. 82–89, 2004.

[24] J. Jin, *The Finite Element Method in Electromagnetics*. New York: John Wiley & Sons, Inc., 2002.

[25] V. Laude, C. Jerez-Hanckes, and S. Ballandras, "Surface Green's function of a piezoelectric halfspace," *IEEE Trans. Ultrason., Ferroelect., Freq. Contr.*, vol. 53, no. 2, pp. 420–428, 2006.

[26] E. Durand, *Electrostatique, Tome II: Problèmes généraux, conducteurs*. Paris: Masson, 1966. (in French)

[27] P. Grisvard, *Elliptic Problems in Nonsmooth Domains*. London: Pitman, 1985.

[28] F. Hecht, O. Pironneau, and A. Le Hyaric, *FreeFem++ v.2.17-2*. Paris: Laboratoire J.-L. Lions, Université Pierre et Marie Curie, Available at http//www.freefem.org Aug. 20, 2008.

[29] K. K. Wong, *Properties of Lithium Niobate*. London: INSPEC, The Institution of Electrical Engineers, 2002.

Carlos F. Jerez-Hanckes (S'03) was born in 1978 in Caracas, Venezuela. He received the B.Sc. and M.Sc. degrees in electrical and industrial engineering with honors from the Pontificia Universidad Católica de Chile, Santiago, Chile, in 2002 and 2005, respectively. In 2005, he also obtained the M.Sc. degree in applied mathematics at the École Polytechnique in Palaiseau, France, where he is currently pursuing his doctoral studies.

In 2001, he was research assistant at the Electronic Devices and Materials laboratory at the University of California, San Diego, USA. His current research interests include fast computational methods for acoustic and electromagnetic waves in complex media, with emphasis on piezoelectric devices, optical waveguides and quasi-periodic structures.

Carlos F. Jerez-Hanckes is a graduate student member of the IEEE UFFC and AP societies.

Vincent Laude (M'00) was born in Bourg-la-Reine, France, in 1968. He received an Engineering Diploma in 1990 from the Ecole Supérieure d'Optique, and a Ph.D. in Physics in 1994 from Paris XI University, both in Orsay, France. He received his Habilitation à Diriger des Recherches from the Université de Franche-Comté in 2002.

From 1995 to 1999, he was a researcher at Thomson-CSF Corporate Research Laboratory (now Thales TRT) in Orsay, France, where he worked on various aspects of optical signal processing, wavefront sensing, and ultrashort laser pulses.

In 2000, he joined Thomson-CSF Microsonics in Sophia-Antipolis, France, to work on surface acoustic wave propagation. At the end of the same year, he joined the Centre National de la Recherche Scientifique in Besançon, France. His research focuses on the propagation of elastic and acoustic waves in micro- and nanostructures, and notably in phononic crystals. He is also interested in highly confined acousto-optical interactions, for instance in phoXonic crytals and fibers. At the FEMTO-ST Institute, he was the head of the LPMO research department for 2006 and 2007, and has been head of the Micro Nano Sciences & Systems research department since 2008.

Vincent Laude is a member of IEEE/UFFC.

Jean-Claude Nédélec was born in 1943 at Briec de l'Odet (Finistère) (France). He was educated at Ingénieur Ecole Polytechnique, Paris, 1963–1966; received his Licence in Mathematics, Sorbonne University, Paris, 1966; and completed his thèse d'état in Mathematics, Sorbonne University, Paris, 1970. He has been employed at E.D.F., Etudes et recherches (1966–1969); Université of Rennes, Professor (1969–1974); and Ecole Polytechnique, Director of the Center for Applied Mathematics (1974–1996). He has been a member of the C.N.U. and C.S.U. (National committee for Universities) (1972–1976, 1984–1986), president of the C.N.U. in mathematics (1991–1999), President of S.M.A.I. (French Society for Applied and Industrial Mathematics) (1987–1990); member of the editorial board of "SIAM Numerical Analysis" (1988–1995); member of the editorial board of "Mathematical Methods in the Applied Sciences" (1977–2001); member of the program committee of ICIAM95; and member of the price committee of CICIAM99. His research interests include optimization and control theory, finite element methods, integral equations, nonlinear hyperbolic equations and theoretical results and numerical techniques for Maxwell equations in electromagnetic problems.

Raphael Lardat is a Mechanical and Electrical Engineer from ENSAM (1988) and received a Ph.D. degree in Computational Fluid Dynamics in 1997 from Paris 6 University. He worked as a research associate in UMIST (University of Manchester Institute of Science and Technology) on turbulent unsteady 3-D flows. He then joined the French state research agency INRIA (Institut National de Recherche en Informatique et Automatisme) where he worked on fluid-structure interaction in large deformation. Following this, he worked for 7 years at TEMEX in applied research for medical ultrasonic probe and SAW (Surface Acoustic Wave) filter applications. He specialized in SAW models and acoustic radiation problems using FEM/BEM (Finite Elements/Boundary Elements) methods. He also worked on modeling and design of passive wireless pressure and temperature SAW sensors. He is now in Thales Underwater Systems working in the advanced underwater acoustic studies group.